Available online at www.sciencedirect.com
SCIENCE DIRECT®
Journal of Computational Physics 196 (2004) 724–750
JOURNAL OF COMPUTATIONAL PHYSICS
www.elsevier.com/locate/jcp

Cubic spline elements for modelling microstructural evolution of materials controlled by solid-state diffusion and grain-boundary migration

H.N. Ch'ng, J. Pan *

School of Engineering (H5), University of Surrey, Guildford GU2 7XH, UK

Received 23 June 2003; received in revised form 21 October 2003; accepted 14 November 2003

Abstract

A new set of finite element formulations are presented in this paper to model surface diffusion, grain-boundary diffusion, grain-boundary migration and their interaction. The new formulations use the classical cubic splines both to represent material interface and to act as shape functions for the migration velocity of the interface. The smoothness of the interface is enforced such that the second order derivatives of the migration velocity is continuous anywhere on the interface. This is achieved by using the cubic spline shape functions and by introducing two new Lagrange terms in the variational principle. The work presented here is a new development to the finite element scheme which was previously developed by Pan, Cocks and their co-workers [Comput. Mater. Sci. 18 (2000) 76; Comput. Mater. Sci. 1 (1993) 95; Acta Mater. 43 (1995) 1395; Proc. Roy. Soc. London A 453 (1997) 2161] for modelling microstructural evolution of materials. The cubic spline elements provide a numerically efficient alternative to the linear elements used by Pan et al. [Proc. Roy. Soc. London A 453 (1997) 2161]. The finite element formulations are verified using a series of test cases for which analytical solutions exist in the literature. A further demonstration case of the co-sintering of two particles of different sizes is provided. The new finite element scheme has made it possible to carry out computer simulations of microstructural evolution using sophisticated and more realistic material models than ever before. The over-simplifications in various existing material models can lead to incorrect predictions. This is dramatically demonstrated in a separate paper in which the finite element scheme is used to investigate the sintering behaviour of large pores [Mech. Mater. (2003)].

Keywords: Microstructural evolution; Finite element; Cubic spline; Solid-state diffusion; Grain-boundary; Computer simulation; Sintering; Model

1. Introduction

In a series of previous works, Pan, Cocks and their co-workers [11,16–18] developed a set of finite element formulations to model microstructural evolution of materials at elevated temperatures. Solid-state

* Corresponding author. Tel.: +44-1483-68-6588/9671; fax: +44-1483-30-6039.
E-mail addresses: h.chng@surrey.ac.uk (H.N. Ch'ng), j.pan@surrey.ac.uk (J. Pan).

0021-9991/$ - see front matter
doi:10.1016/j.jcp.2003.11.012

diffusion and grain-boundary migration were considered as the underlying mechanisms for the evolution. The finite element scheme has been used to study a range of material behaviour including creep failure of engineering alloys [6], superplasticity [16] and sintering of powder compacts [11,20]. These numerical studies have helped to improve our understanding of materials behaviour at elevated temperatures [8,15]. Similar efforts have been made by Suo and co-workers [21–23], Zhang, Schneibel and co-workers [24,25] and some recent progress in particular on modelling surface diffusion can be found in [1,2,13].

In all the previous works by Pan, Cocks and their co-workers, the material interfaces (grain-boundaries and free surfaces) were represented by a series of straight elements and a linear distribution of the interfacial velocity was assumed over each element. These linear elements are numerically effective but computationally inefficient, which became apparent as they were used to model problems on large scales. Recently Cocks and Gill [5] used the classical cubic spline to model grain-growth. In this paper we further develop their concept and present a set of cubic spline finite elements to model grain-boundary diffusion, surface diffusion and grain-boundary migration, respectively. The grain-boundaries and free surfaces are represented using cubic splines and the same cubic splines are also used as the shape functions for the migration velocity of the interfaces. Similar to the higher-order elements in the classical finite element method, the cubic spline elements make it possible to use only a few elements to represent a grain-boundary or a free surface. Unlike the ordinary high-order elements, however, we also enforce the smoothness of the interfaces by introducing two new Lagrange multipliers in the variational principle which force the first and second derivatives of the migration velocity to be continuous across all the finite element nodes on each interface. This filters out any high frequency oscillation during the time integration and accelerates the numerical solution dramatically.

The cubic spline elements are tested using a series of numerical examples for which analytical solutions exist in the literature. As a demonstration example, the finite element scheme is used to numerically simulate the co-sintering process of two cylindrical particles of different sizes in which grain-boundary diffusion, surface diffusion and grain-boundary migration are strongly coupled. The cubic spline formulations, combined with a time integration algorithm, form a numerical technique for computer simulation of morphological evolution at the level of grain size in porous polycrystalline materials. The numerical scheme has made it possible to study the microstructural evolution in polycrystalline materials at an unprecedented scale. This is demonstrated in a separate paper in which the numerical scheme is used to study the sintering behaviour of large pores which are embedded in a matrix of irregular grains [19].

2. The modified variational principle

We consider a two-dimensional system consisting of a grain-boundary network, Γ_{gb}, intersected by internal and/or external free surfaces, Γ_s. Fig. 1 shows a small part of the microstructure which consists of two grains, a grain-boundary and two free surfaces.

Along part of the external boundary of the system, Γ_F, an external distributed force $\boldsymbol{F}$ is applied. The total potential energy E of the system is

$$E = \int_{\Gamma_{gb}} \gamma_{gb}\,\mathrm{d}\Gamma + \int_{\Gamma_s} \gamma_s\,\mathrm{d}\Gamma - \int_{\Gamma_F} \boldsymbol{F}\cdot\boldsymbol{U}\,\mathrm{d}\Gamma, \tag{1}$$

where γ_{gb} and γ_s are specific energies for grain-boundary and free surface, respectively, and $\boldsymbol{U}$ is the displacement of Γ_F with respect to a reference configuration. The system evolves to reduce E. The grains are assumed to be rigid and only three processes that dissipate energy are considered: grain-boundary diffusion, surface diffusion and grain-boundary migration. The diffusive flux, defined as volume of matter flowing along the interface across unit slab thickness of the interface per unit time, is referred to as j_{gb} for grain-boundary diffusion and j_s for surface diffusion. The migrating velocity of a grain-boundary is referred to as v_m.

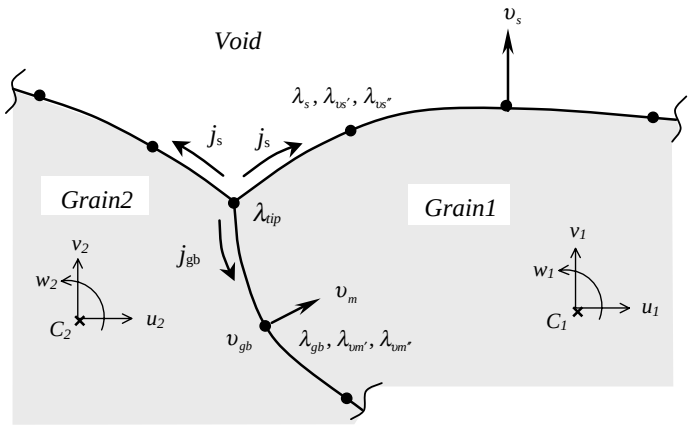

Fig. 1. A small part of the microstructure considered in this paper. The interfaces are discretised using the degrees of freedom shown in the figure which include: v_s, the migration velocity of a free surface; v_m, the migration velocity of a grain-boundary; v_{gb}, the separation velocity of a grain-boundary due to grain-boundary diffusion; u_1, v_1, ω_1, u_2, v_2, ω_2 the translational and rotational velocities of the two grains defined at C_1 and C_2, respectively; j_s and j_{gb}, the diffusive fluxes along the free surface and grain-boundary respectively; λ_s and λ_{gb}, the Lagrange multipliers to force the continuity of the diffusive fluxes along the surface and grain-boundary, respectively; $\lambda_{v_s'}$ and $\lambda_{v_s''}$ the Lagrange multipliers to force the continuity of the first and second derivatives of surface migration velocity; $\lambda_{v_m'}$ and $\lambda_{v_m''}$ the Lagrange multipliers to force the continuity of the first and second derivatives of grain-boundary migration velocity and λ_{tip} the Lagrange multiplier to force matter conservation at the triple junction.

The evolution of the grain-boundaries and free surfaces is governed by a variational principle, that is, among all the possible diffusive fluxes and migration velocities which satisfy matter conservation, the true fluxes and velocities make a functional Π minimum,

$$\Pi = \int_{\Gamma_{gb}} \frac{1}{2M_{gb}} j_{gb}^2 \, d\Gamma + \int_{\Gamma_s} \frac{1}{2M_s} j_s^2 \, d\Gamma + \int_{\Gamma_{gb}} \frac{1}{2M_m} v_m^2 \, d\Gamma + \frac{dE}{dt}, \tag{2}$$

where M_{gb}, M_s and M_m are the mobilities associated with grain-boundary diffusion, surface diffusion and grain-boundary migration, respectively. Needleman and Rice [14] developed the original version of this variational principle. They considered grain-boundary diffusion and power law creep. Suo and Wang [23], Cocks and Gill [5], Cocks [4] and Pan et al. [18] later extended it to include surface diffusion, lattice diffusion and grain-boundary migration. These authors have shown that $\delta\Pi = 0$ leads to the linear kinetic laws for the three processes, respectively [9,10]:

$$j_{gb} = M_{gb} \frac{\partial \sigma}{\partial s}, \tag{3}$$

$$j_s = M_s \frac{\partial(\gamma_s \kappa_s)}{\partial s} \tag{4}$$

and

$$v_m = M_m \gamma_{gb} \kappa_{gb}, \tag{5}$$

in which σ is the stress normal to the grain-boundary, κ_s and κ_{gb} are the principal curvatures of the free surface and grain-boundary, respectively, and s is a local co-ordinate along either a grain-boundary or a free surface. Apart from the three kinetic laws, $\delta\Pi = 0$ also leads to the equilibrium between the grain-boundary stresses, the surface tension and the externally applied forces, and the equilibrium between the interfacial

tensions at all the junctions between the interfaces. Usual boundary conditions for diffusive fluxes, applied forces and boundary velocities have to be specified to fully define the problem mathematically.

When constructing numerical solutions, it is often difficult to satisfy matter conservation everywhere. Cocks [3] introduced a Lagrange term, $\sum \lambda_j(\sum j)$, to enforce matter conservation in the variational sense where it is violated. The outer summation is over all the locations where matter conservation is violated and the inner summation is over all the fluxes flowing into such a location. This has been proven to be a very effective technique in the previous work by Pan, Cocks and their co-workers [3–5,11,17,18]. Here, we extend this technique further to enforce the smoothness of the migrating velocity of an interface in the numerical solution. As mentioned in Section 1, it is desirable to develop a high-order element so that fewer elements can be used and the interface can evolve in a smooth manner. However, simply using a high-order shape function in each element can lead to oscillation of the numerical solution. We therefore introduce two more Lagrange terms in the variational principle to enforce the continuity of the first and second derivatives of the migrating velocity across all the finite element nodes on a single grain-boundary or free surface. The modified functional Π^* is given by

$$\Pi^* = \int_{\Gamma_{\mathrm{gb}}} \frac{1}{2M_{\mathrm{gb}}} j_{\mathrm{gb}}^2 \,\mathrm{d}\Gamma + \int_{\Gamma_{\mathrm{s}}} \frac{1}{2M_{\mathrm{s}}} j_{\mathrm{s}}^2 \,\mathrm{d}\Gamma + \int_{\Gamma_{\mathrm{gb}}} \frac{1}{2M_{\mathrm{m}}} v_{\mathrm{m}}^2 \,\mathrm{d}\Gamma + \frac{\mathrm{d}E}{\mathrm{d}t} + \sum \lambda_j \Big(\sum j \Big) + \sum \lambda_{v'} \Big(\sum v' \Big) + \sum \lambda_{v''} \Big(\sum v'' \Big), \tag{6}$$

in which v represents the migrating velocity of the interface, v' and v'' the first and second derivatives of v with respect to the local coordinates along the interface, and $\lambda_{v'}$ and $\lambda_{v''}$ the Lagrange multipliers at any junction of two connecting elements except for the triple junctions. The outer summations of the two new terms are over all the finite element nodes expect for the triple grain-boundary junctions and where the grain-boundaries meet the free surfaces. The inner summations are over the two joining elements. In the later sections, the migrating velocity of the interface will be referred to as v_{s} for the free surface, and v_{m} for the grain-boundary. The two newly-introduced Lagrange terms guarantee the smoothness of the interface as it evolves and are consistent with the cubic spline shape functions used to represent the migration velocity which will be introduced in Sections 4 and 5.

3. Representing an interface using cubic spline elements

As shown in Fig. 2, an interface can be represented using the classical cubic spline. The interface is divided into n elements. For the jth element we have

$$x_j = a_{x_j} + b_{x_j}(S - S_j) + c_{x_j}(S - S_j)^2 + d_{x_j}(S - S_j)^3 \tag{7}$$

and

$$y_j = a_{y_j} + b_{y_j}(S - S_j) + c_{y_j}(S - S_j)^2 + d_{y_j}(S - S_j)^3, \tag{8}$$

in which a_j, b_j, c_j and d_j are the cubic spline coefficients for element j, and S is a curvilinear coordinate along the interface with its origin at the left end of the interface.

Fig. 3 shows an isolated element. The global coordinates of the two nodes of the element are referred to as $x_{1,j}, y_{1,j}$ and $x_{2,j}, y_{2,j}$. For each element, a non-dimensionalised local coordinate ζ is introduced as shown in the figure. The origin of ζ is located at the mid-point of the element and it is normalised by the half-length of the element, S_{e_j}, so that $\zeta = -1$ at the left node and $\zeta = 1$ at the right node. Replacing the global coordinate by the local coordinate ζ, we have

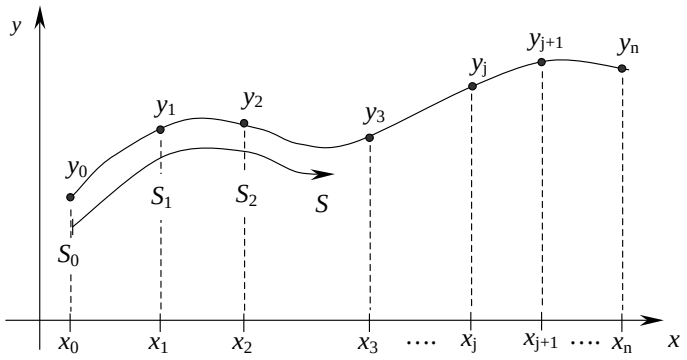

Fig. 2. Representing an interface using cubic spline elements, where S is a local coordinate along the interface. Note that there are n intervals and $n+1$ data points.

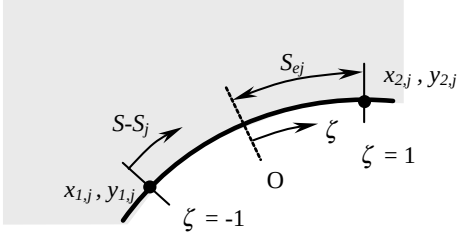

Fig. 3. The local coordinate system of an isolated element.

$$S - S_j = S_{e_j}(1+\zeta). \tag{9}$$

It is obvious that $a_{x_j} = x_{1,j}$ and $a_{y_j} = y_{1,j}$. Furthermore, b_{x_j} and b_{y_j} can be expressed as

$$b_{x_j} = \frac{1}{2S_{e_j}}x_{2,j} - \frac{1}{2S_{e_j}}x_{1,j} - 2S_{e_j}c_{x_j} - 4S_{e_j}^2 d_{x_j}$$

and

$$b_{y_j} = \frac{1}{2S_{e_j}}y_{2,j} - \frac{1}{2S_{e_j}}y_{1,j} - 2S_{e_j}c_{y_j} - 4S_{e_j}^2 d_{y_j},$$

respectively. By substituting the above expressions for a_{x_j}, a_{y_j}, b_{x_j}, b_{y_j} and $(S - S_j)$ into Eqs. (7) and (8), the cubic spline equations of the interface element can be re-written into a typical finite element format as following:

$$x_j(\zeta) = [N_1(\zeta)\ N_2(\zeta)\ N_3(\zeta)\ N_4(\zeta)]\begin{bmatrix} x_{1,j} \\ x_{2,j} \\ c_{x_j} \\ d_{x_j} \end{bmatrix} \tag{10}$$

and

$$y_j(\zeta) = [N_1(\zeta)\ N_2(\zeta)\ N_3(\zeta)\ N_4(\zeta)]\begin{bmatrix} y_{1,j} \\ y_{2,j} \\ c_{x_j} \\ d_{x_j} \end{bmatrix}, \tag{11}$$

in which $N_1(\zeta)$, $N_2(\zeta)$, $N_3(\zeta)$ and $N_4(\zeta)$ are the shape functions, which are given by

$$\left.\begin{aligned} N_1(\zeta) &= \tfrac{1}{2}(1-\zeta),\\ N_2(\zeta) &= \tfrac{1}{2}(1+\zeta),\\ N_3(\zeta) &= S_{e_j}^2(\zeta^2-1),\\ N_4(\zeta) &= S_{e_j}^3[(1+\zeta)^3-4(1+\zeta)]. \end{aligned}\right\} \tag{12}$$

The parameters c_{x_j}, c_{y_j} and d_{x_j}, d_{y_j} can be uniquely determined from the nodal coordinates using the classical cubic spline procedure by enforcing the continuity of the first and the second derivatives of x and y with respect to S across all the nodes and by considering the end conditions at both ends of the interface.

4. A cubic spline element for surface diffusion

For surface diffusion, the surface migrates in the direction normal to the surface as matter is removed from or added to a particular part of the surface by the diffusion process. Let υ_s represent the migration velocity, which is taken as positive if the surface migrates toward the space, and j_s represent the diffusive flux along the surface. Matter conservation requires that

$$\frac{\partial j_s}{\partial S} + \upsilon_s = 0, \tag{13}$$

in which S is the same local coordinate along the surface used in the previous section.

For each element, we express the migration velocity υ_s in terms of the same shape functions as those used for the surface itself in the previous section, i.e., we assume

$$\upsilon_s(\zeta) = [N_1(\zeta)\ N_2(\zeta)\ N_3(\zeta)\ N_4(\zeta)] \begin{bmatrix} \upsilon_{s,1} \\ \upsilon_{s,2} \\ c_{\upsilon_s} \\ d_{\upsilon_s} \end{bmatrix}, \tag{14}$$

in which $\upsilon_{s,1}$ and $\upsilon_{s,2}$ are the two nodal velocities at the two ends of the element, c_{υ_s} and d_{υ_s} are the cubic spline coefficients for υ_s, and $N_1(\zeta)$, $N_2(\zeta)$, $N_3(\zeta)$ and $N_4(\zeta)$ are the shape functions defined by Eq. (12). $\upsilon_{s,1}$, $\upsilon_{s,2}$, c_{υ_s} and d_{υ_s} are the unknown degrees of freedom of the free surface element (Fig. 4).

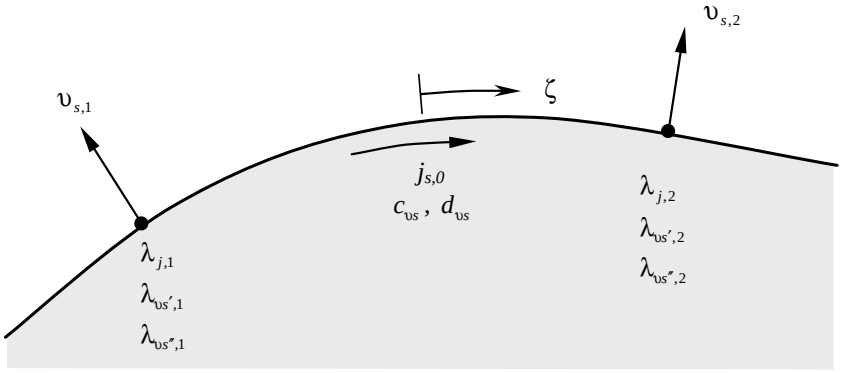

Fig. 4. A surface diffusion element showing all the degrees of freedom.

From Eq. (13), we have

$$j_s(\zeta) = -S_e \int_0^{\zeta} \upsilon_s(\zeta)\,d\zeta + j_{s,0}, \tag{15}$$

where $j_{s,0}$ is the diffusive flux across the origin of the local coordinate. Substituting Eq. (14) into Eq. (15), we obtain

$$j_s(\zeta) = [\psi_1(\zeta)\ \psi_2(\zeta)\ \psi_3(\zeta)\ \psi_4(\zeta)\ 1] \begin{bmatrix} \upsilon_{s,1} \\ \upsilon_{s,2} \\ c_{\upsilon_s} \\ d_{\upsilon_s} \\ j_{s,0} \end{bmatrix}, \tag{16}$$

in which

$$\left.\begin{aligned} \psi_1(\zeta) &= -\tfrac{S_e}{2}\left(\zeta - \tfrac{1}{2}\zeta^2\right), \\ \psi_2(\zeta) &= -\tfrac{S_e}{2}\left(\zeta + \tfrac{1}{2}\zeta^2\right), \\ \psi_3(\zeta) &= -S_e^3\left(\tfrac{1}{3}\zeta^3 - \zeta\right), \\ \psi_4(\zeta) &= -S_e^4\left[\tfrac{1}{4}(1+\zeta)^4 - 2\zeta^2 - 4\zeta\right]. \end{aligned}\right\} \tag{17}$$

The contribution of the surface element to the functional Π^* can be calculated by substituting expression (16) into the corresponding term in functional Π^* given by Eq. (6):

$$\int_{\Gamma_e} \frac{1}{2M_s} j_s^2\,d\Gamma = \frac{S_e}{2M_s}\int_{-1}^{1} j_s^2(\zeta)\,d\zeta = \frac{1}{2}[\upsilon_{s,1}\ \upsilon_{s,2}\ c_{\upsilon_s}\ d_{\upsilon_s}\ j_{s,0}][K_s] \begin{bmatrix} \upsilon_{s,1} \\ \upsilon_{s,2} \\ c_{\upsilon_s} \\ d_{\upsilon_s} \\ j_{s,0} \end{bmatrix}, \tag{18}$$

where $[K_s]$ is a 5×5 viscosity matrix for surface diffusion. The detailed expression for $[K_s]$ can be found in Appendix A.

At each node, matter conservation for the diffusive flux is not guaranteed by expression (16). In the numerical solution, the matter conservation is enforced by the corresponding Lagrange multiplier term in the variational principle. Furthermore, the continuity of the first and second derivatives of the velocity across each node is enforced by two newly introduced Lagrange terms as explained in Section 2. The contribution of each element to the three Lagrange terms of the functional Π^* can be written as

$$\frac{1}{2}\left[\lambda_{\upsilon_s',2}\ \lambda_{\upsilon_s',1}\ \lambda_{\upsilon_s'',2}\ \lambda_{\upsilon_s'',1}\ \lambda_{j,2}\ \lambda_{j,1}\right] \begin{bmatrix} \upsilon_s'(1) \\ -\upsilon_s'(-1) \\ \upsilon_s''(1) \\ -\upsilon_s''(-1) \\ j_s(1) \\ -j_s(-1) \end{bmatrix} = \frac{1}{2}\left[\lambda_{\upsilon_s',2}\ \lambda_{\upsilon_s',1}\ \lambda_{\upsilon_s'',2}\ \lambda_{\upsilon_s'',1}\ \lambda_{j,2}\ \lambda_{j,1}\right][C_s] \begin{bmatrix} \upsilon_{s,1} \\ \upsilon_{s,2} \\ c_{\upsilon_s} \\ d_{\upsilon_s} \\ j_{s,0} \end{bmatrix}, \tag{19}$$

where $[C_s]$ is a 6×5 complementary matrix. The detailed elements in $[C_s]$ are given in Appendix A. The total contribution of the current element to the functional, Π^*, can be combined into the following form:

$$\frac{1}{2}\left[\upsilon_{s,1}\ \upsilon_{s,2}\ c_{\upsilon_s}\ d_{\upsilon_s}\ j_{s,0}\ \lambda_{\upsilon_s',2}\ \lambda_{\upsilon_s',1}\ \lambda_{\upsilon_s'',2}\ \lambda_{\upsilon_s'',1}\ \lambda_{j,2}\ \lambda_{j,1}\right] \begin{bmatrix} [K_s] & [C_s]^T \\ [C_s] & 0 \end{bmatrix} \begin{bmatrix} \upsilon_{s,1} \\ \vdots \\ \lambda_{j,1} \end{bmatrix} = \frac{1}{2}[U_s]^T[A_s][U_s], \tag{20}$$

in which $[U_s]$ is the vector of elemental unknowns and $[A_s]$ is the generalised viscosity matrix of the element under consideration.

The contribution from the current element to the term dE/dt of the functional Π^* can be calculated as

$$S_e\gamma_s\int_{-1}^{1}\left\{\kappa_s(\zeta)[N_1(\zeta)\ N_2(\zeta)\ N_3(\zeta)\ N_4(\zeta)]\begin{bmatrix}\upsilon_{s,1}\\ \upsilon_{s,2}\\ c_{\upsilon_s}\\ d_{\upsilon_s}\end{bmatrix}\right\}d\zeta=[F_s]\begin{bmatrix}\upsilon_{s,1}\\ \upsilon_{s,2}\\ c_{\upsilon_s}\\ d_{\upsilon_s}\end{bmatrix}, \tag{21}$$

in which γ_s is the specific free surface energy and κ_s is the curvature of the local element which can be calculated from Eqs. (7) and (8),

$$\kappa_s=\frac{\dot{x}\ddot{y}-\dot{y}\ddot{x}}{\left(\dot{x}^2+\dot{y}^2\right)^{3/2}}, \tag{22}$$

where a dot represents d/dS. $[F_s]$ is referred to as the elementary force matrix for surface diffusion. Gauss quadrature integration is used to integrate the complicated expression in Eq. (21) to obtain $[F_s]$.

The contribution from a surface element to the function Π^* can now be combined as

$$\frac{1}{2}[U_s]^T[A_s][U_s]+[F_s]\begin{bmatrix}\upsilon_{s,1}\\ \upsilon_{s,2}\\ c_{\upsilon_s}\\ d_{\upsilon_s}\end{bmatrix}, \tag{23}$$

where a free surface meets a grain-boundary, the above equations are not valid for two reasons. The first is that the velocity of the triple point, as shown in Fig. 5 is no longer normal to any of the interfaces joining the junction. At this junction, the equilibrium condition between the surface and grain-boundary tensions leads to a discontinuity in the normal to the surface. Both the magnitude and the direction of the velocity of the junction have to be determined from the numerical solution. The second reason is that it is inappropriate to force the continuity of the first and second derivatives of the migration velocity at the triple junction, hence the two newly introduced Lagrange multiplier terms do not apply to the junction.

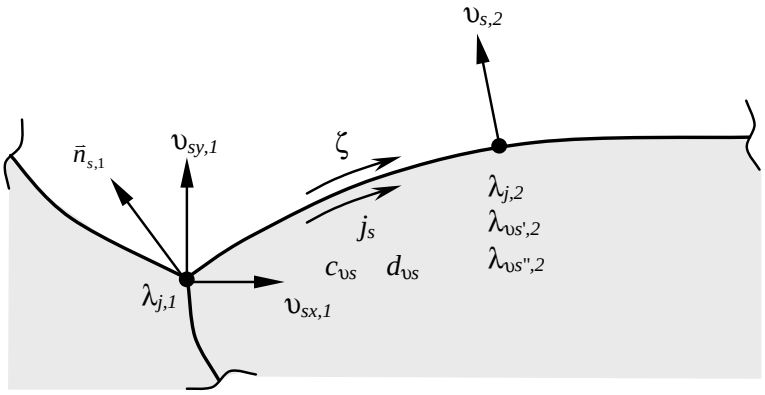

Fig. 5. A special surface diffusion element which joins a grain-boundary at its left end. Both the direction and magnitude of the velocity of the triple junction have to be determined from the finite element solution. The variational principle guarantees the balance of the interfacial tensions at the triple point so that the correct dihedral angle is maintained by the numerical solution of the velocities of the three elements joining at the triple point.

We decompose the velocity of the triple junction into its x- and y-components in the global coordinate system and refer to them as υ_{s_x} and υ_{s_y}, respectively. Fig. 5 shows a special surface diffusion element located at the right side of a triple junction. The migration velocity of the special element can then be written as

$$\upsilon_{\mathrm{s}}(\zeta) = \begin{bmatrix} n_{s_x,1}N_1(\zeta) & n_{s_y,1}N_1(\zeta) & N_2(\zeta) & N_3(\zeta) & N_4(\zeta) \end{bmatrix} \begin{bmatrix} \upsilon_{s_x,1} \\ \upsilon_{s_y,1} \\ \upsilon_{\mathrm{s},2} \\ c_{\upsilon_{\mathrm{s}}} \\ d_{\upsilon_{\mathrm{s}}} \end{bmatrix}, \tag{24}$$

in which $n_{s_x,1}$ and $n_{s_y,1}$ are the x- and y-components of the normal $\vec{n}_{\mathrm{s},1}$ at the left end of the special element; $N_1(\zeta)$, $N_2(\zeta)$, $N_3(\zeta)$ and $N_4(\zeta)$ are the shape functions given by Eq. (12). Following the similar procedure used for the normal surface element, we obtain the contribution from the special surface diffusion element to the functional Π^* as

$$\frac{1}{2}\begin{bmatrix} \upsilon_{s_x,1} & \upsilon_{s_y,1} & \upsilon_{\mathrm{s},2} & c_{\upsilon_{\mathrm{s}}} & d_{\upsilon_{\mathrm{s}}} & j_{\mathrm{s},0} & \lambda_{\upsilon'_s,2} & \lambda_{\upsilon''_s,2} & \lambda_{j,2} & \lambda_{j,1} \end{bmatrix} \begin{bmatrix} \begin{bmatrix} K^*_{\mathrm{s}} \\ C^*_{\mathrm{s}} \end{bmatrix} & \begin{bmatrix} C^*_{\mathrm{s}} \end{bmatrix}^{\mathrm{T}} \\ 0 \end{bmatrix} \begin{bmatrix} \upsilon_{s_x,1} \\ \vdots \\ \lambda_{j,1} \end{bmatrix} = \frac{1}{2}\left[U^*_{\mathrm{s}}\right]^{\mathrm{T}}\left[A^*_{\mathrm{s}}\right]\left[U^*_{\mathrm{s}}\right], \tag{25}$$

in which $[U^*_{\mathrm{s}}]$ and $[A^*_{\mathrm{s}}]$ are the vector of unknowns and the generalised viscosity matrix, respectively, of the special element. $[K^*_{\mathrm{s}}]$ and $[C^*_{\mathrm{s}}]$ are the 6×6 viscosity matrix and 4×6 complementary matrix for the special element, respectively. The details of these two matrixes are provided in Appendix A.

The contribution of the special element to $\mathrm{d}E/\mathrm{d}t$ of the functional Π^* is

$$S_{\mathrm{e}}\gamma_{\mathrm{s}}\int_{-1}^{1}\left\{\kappa_{\mathrm{s}}(\zeta)\begin{bmatrix} n_{s_x,1}N_1(\zeta) & n_{s_y,1}N_1(\zeta) & N_2(\zeta) & N_3(\zeta) & N_4(\zeta) \end{bmatrix}\begin{bmatrix} \upsilon_{s_x,1} \\ \upsilon_{s_y,1} \\ \upsilon_{\mathrm{s},2} \\ c_{\upsilon_{\mathrm{s}}} \\ d_{\upsilon_{\mathrm{s}}} \end{bmatrix}\right\}\mathrm{d}\zeta = \begin{bmatrix} F^*_{\mathrm{s}} \end{bmatrix}\begin{bmatrix} \upsilon_{s_x,1} \\ \upsilon_{s_y,1} \\ \upsilon_{\mathrm{s},2} \\ c_{\upsilon_{\mathrm{s}}} \\ d_{\upsilon_{\mathrm{s}}} \end{bmatrix}, \tag{26}$$

in which $[F^*_{\mathrm{s}}]$ is the force matrix of the special element. The total contribution to the functional Π^* from all the free surfaces is the summation of Eq. (23) for all the ordinary surface elements and Eqs. (25) and (26) for all the special elements which meet the grain-boundaries.

5. A cubic spline element for grain-boundary migration

The finite element formulation for grain-boundary migration is similar to that for surface diffusion. A grain-boundary is represented by a set of cubic spline elements. Considering an isolated grain-boundary migration element shown in Fig. 6, the migration velocity of the grain-boundary, υ_{m}, can be expressed in terms of the same cubic spline shape functions used for surface diffusion:

$$\upsilon_{\mathrm{m}}(\zeta) = \begin{bmatrix} N_1(\zeta) & N_2(\zeta) & N_3(\zeta) & N_4(\zeta) \end{bmatrix}\begin{bmatrix} \upsilon_{\mathrm{m},1} \\ \upsilon_{\mathrm{m},2} \\ c_{\upsilon_{\mathrm{m}}} \\ d_{\upsilon_{\mathrm{m}}} \end{bmatrix}, \tag{27}$$

in which $c_{\upsilon_{\mathrm{m}}}$ and $d_{\upsilon_{\mathrm{m}}}$ are the cubic spline coefficients; $\upsilon_{\mathrm{m},1}$ and $\upsilon_{\mathrm{m},2}$ are the migration velocities of the two nodes; and $N_1(\zeta)$, $N_2(\zeta)$, $N_3(\zeta)$ and $N_4(\zeta)$ are the shape functions given by Eq. (12). The contribution of the current element to the functional Π^* is then

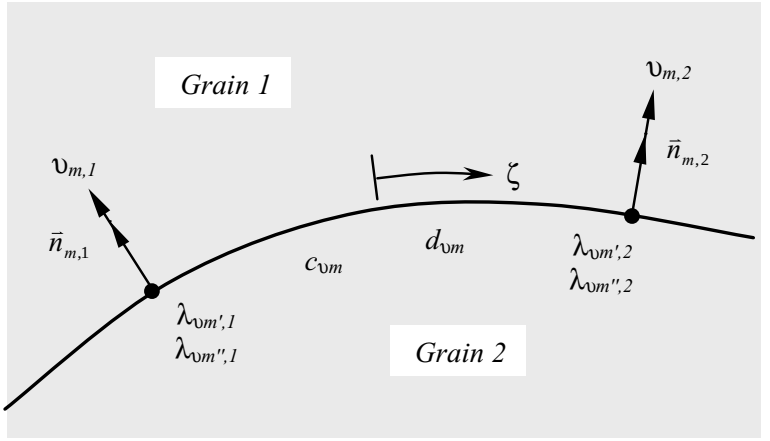

Fig. 6. A grain-boundary migration element showing all the degrees of freedom.

$$\int_{\Gamma_e} \frac{1}{2M_m} \upsilon_m^2 \, d\Gamma = \frac{S_e}{2M_m} \int_{-1}^{1} \upsilon_m^2(\zeta) \, d\zeta = \frac{1}{2} [\upsilon_{m,1} \ \upsilon_{m,2} \ c_{\upsilon_m} \ d_{\upsilon_m}][K_m] \begin{bmatrix} \upsilon_{m,1} \\ \upsilon_{m,2} \\ c_{\upsilon_m} \\ d_{\upsilon_m} \end{bmatrix}, \tag{28}$$

where $[K_m]$ is a 4×4 viscosity matrix for grain-boundary migration. The details of $[K_m]$ are provided in Appendix A.

The continuity of the first and second derivatives of the migration velocity is enforced by using Lagrange multipliers, $\lambda_{\upsilon'_m}$ and $\lambda_{\upsilon''_m}$. The contribution of each element to the Lagrange terms of functional Π^* is

$$\frac{1}{2} \begin{bmatrix} \lambda_{\upsilon'_m,2} & \lambda_{\upsilon'_m,1} & \lambda_{\upsilon''_m,2} & \lambda_{\upsilon''_m,1} \end{bmatrix} \begin{bmatrix} \upsilon'_m(1) \\ -\upsilon'_m(-1) \\ \upsilon''_m(1) \\ -\upsilon''_m(-1) \end{bmatrix} = \frac{1}{2} \begin{bmatrix} \lambda_{\upsilon'_m,2} & \lambda_{\upsilon'_m,1} & \lambda_{\upsilon''_m,2} & \lambda_{\upsilon''_m,1} \end{bmatrix} [C_m] \begin{bmatrix} \upsilon_{m,1} \\ \upsilon_{m,2} \\ c_{\upsilon_m} \\ d_{\upsilon_m} \end{bmatrix}, \tag{29}$$

where $[C_m]$ is a 4×4 complementary matrix. The details of $[C_m]$ are given in Appendix A.

The contribution from the current element to the term dE/dt of the functional Π^* is simply

$$S_e \gamma_{gb} \int_{-1}^{1} \left\{ \kappa_{gb}(\zeta) [N_1(\zeta) \ N_2(\zeta) \ N_3(\zeta) \ N_4(\zeta)] \begin{bmatrix} \upsilon_{m,1} \\ \upsilon_{m,2} \\ c_{\upsilon_m} \\ d_{\upsilon_m} \end{bmatrix} \right\} d\zeta = [F_m] \begin{bmatrix} \upsilon_{m,1} \\ \upsilon_{m,2} \\ c_{\upsilon_m} \\ d_{\upsilon_m} \end{bmatrix}, \tag{30}$$

where κ_{gb} is the curvature of the grain-boundary and γ_{gb} is the specific grain-boundary energy. $[F_m]$ is referred to as the elementary force matrix for grain-boundary migration.

Combining Eqs. (28)–(30) gives the contribution of current element to the functional Π^* which is

$$\frac{1}{2} [\upsilon_{m,1} \ \upsilon_{m,2} \ c_{\upsilon_m} \ d_{\upsilon_m} \ \lambda_{\upsilon'_m,2} \ \lambda_{\upsilon'_m,1} \ \lambda_{\upsilon''_m,2} \ \lambda_{\upsilon''_m,1}] \begin{bmatrix} [K_m] & [C_m]^T \\ [C_m] & 0 \end{bmatrix} \begin{bmatrix} \upsilon_{m,1} \\ \vdots \\ \lambda_{\upsilon''_m,1} \end{bmatrix} + [F_m] \begin{bmatrix} \upsilon_{m,1} \\ \upsilon_{m,2} \\ c_{\upsilon_m} \\ d_{\upsilon_m} \end{bmatrix}$$

$$= \frac{1}{2} [U_m]^T [A_m][U_m] + [F_m] \begin{bmatrix} \upsilon_{m,1} \\ \upsilon_{m,2} \\ c_{\upsilon_m} \\ d_{\upsilon_m} \end{bmatrix}, \tag{31}$$

in which $[U_{\mathrm{m}}]$ is the vector of element unknowns and $[A_{\mathrm{m}}]$ is the generalised viscosity matrix for the element under consideration.

Likewise, Eqs. (30) and (31) are not valid where the grain-boundary meets either other grain-boundaries or a free surface. Fig. 7 shows an example where a grain-boundary meets a pore surface. Once again, we decompose the migration velocity of the junction into two components, $\upsilon_{\mathrm{m}_x,2}$ and $\upsilon_{\mathrm{m}_y,2}$. In fact, both of them are not new but the same as $\upsilon_{\mathrm{s}_x,1}$ and $\upsilon_{\mathrm{s}_y,1}$, which were introduced earlier while developing the special element for surface diffusion. The migration velocity, υ_{m} takes the similar form as Eq. (24),

$$\upsilon_{\mathrm{m}}(\zeta) = [N_1(\zeta)\ n_{\mathrm{m}_x,2}N_2(\zeta)\ n_{\mathrm{m}_y,2}N_2(\zeta)\ N_3(\zeta)\ N_4(\zeta)] \begin{bmatrix} \upsilon_{\mathrm{m},1} \\ \upsilon_{\mathrm{m}_x,2} \\ \upsilon_{\mathrm{m}_y,2} \\ c_{\upsilon_{\mathrm{m}}} \\ d_{\upsilon_{\mathrm{m}}} \end{bmatrix}. \tag{32}$$

Following the similar procedure, we obtain the contribution of the special grain-boundary migration element to the functional Π^* as

$$\frac{1}{2}[\upsilon_{\mathrm{m},1}\ \upsilon_{\mathrm{m}_x,2}\ \upsilon_{\mathrm{m}_y,2}\ c_{\upsilon_{\mathrm{m}}}\ d_{\upsilon_{\mathrm{m}}}\ \lambda_{\upsilon'_{\mathrm{m}},1}\ \lambda_{\upsilon''_{\mathrm{m}},1}] \begin{bmatrix} [K^*_{\mathrm{m}}] & [C^*_{\mathrm{m}}]^{\mathrm{T}} \\ [C^*_{\mathrm{m}}] & 0 \end{bmatrix} \begin{bmatrix} \upsilon_{\mathrm{m},1} \\ \vdots \\ \lambda_{\upsilon_{\mathrm{m}},1} \end{bmatrix} = \frac{1}{2}[U^*_{\mathrm{m}}]^{\mathrm{T}}[A^*_{\mathrm{m}}][U^*_{\mathrm{m}}], \tag{33}$$

in which $[U^*_{\mathrm{m}}]$ and $[A^*_{\mathrm{m}}]$ are the vector of unknowns and the generalised viscosity matrix, respectively, for the special element. $[K^*_{\mathrm{m}}]$ and $[C^*_{\mathrm{m}}]$ are the 5×5 viscosity matrix and the 2×5 complementary matrix from the special element, respectively. The details of $[K^*_{\mathrm{m}}]$ and $[C^*_{\mathrm{m}}]$ can be found in Appendix A.

The contribution of the special element to $\mathrm{d}E/\mathrm{d}t$ of the functional Π^* is given by

$$S_{\mathrm{e}}\gamma_{\mathrm{gb}}\int_{-1}^{1}\left\{\kappa_{\mathrm{gb}}(\zeta)[N_1(\zeta)\ n_{\mathrm{m}_x,2}N_2(\zeta)\ n_{\mathrm{m}_y,2}N_2(\zeta)\ N_3(\zeta)\ N_4(\zeta)] \begin{bmatrix} \upsilon_{\mathrm{m},1} \\ \upsilon_{\mathrm{m}_x,2} \\ \upsilon_{\mathrm{m}_y,2} \\ c_{\upsilon_{\mathrm{m}}} \\ d_{\upsilon_{\mathrm{m}}} \end{bmatrix}\right\}\mathrm{d}\zeta = [F^*_{\mathrm{m}}] \begin{bmatrix} \upsilon_{\mathrm{m},1} \\ \upsilon_{\mathrm{m}_x,2} \\ \upsilon_{\mathrm{m}_y,2} \\ c_{\upsilon_{\mathrm{m}}} \\ d_{\upsilon_{\mathrm{m}}} \end{bmatrix}, \tag{34}$$

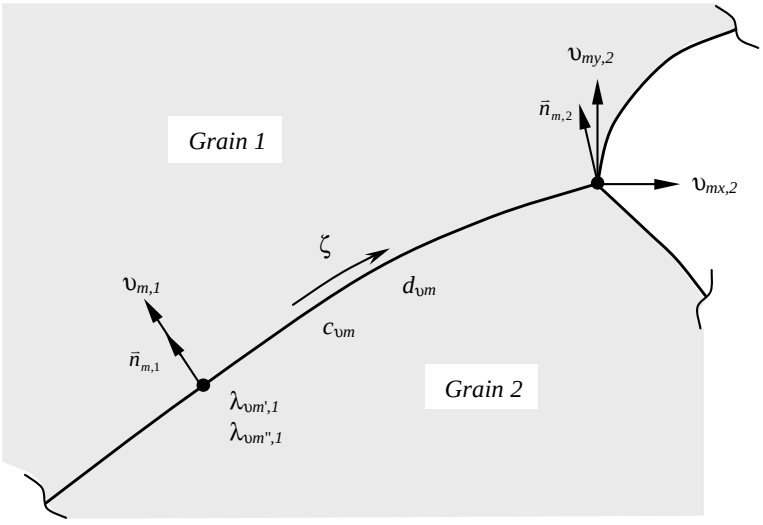

Fig. 7. A special grain-boundary migration element joining a triple junction at its right end. Also see the note in the caption for Fig. 5.

in which $[F_m^*]$ is the force matrix of the special element. The total contribution to the functional Π^* from all the grain-boundaries is the summation of Eq. (31) for all the ordinary grain-boundary elements and Eqs. (33) and (34) for all the special elements which meet either other grain-boundaries or a free surfaces.

6. A cubic spline element for grain-boundary diffusion

As atoms diffuse along a grain-boundary, matter is either removed from, or deposited onto, a particular location of a grain-boundary. Such matter redistribution leads to stresses in the grains on either side of the grain-boundary and causes deformation of the grains. The grains can deform either elastically [23] or plastically [14] depending on the level of the stress and the time frame of the process. The elastic energy can also contribute to the driving force for solid-state diffusion and become an important part of the problem [23]. In a wide range of practical problems, however, the diffusion process can quickly release the stresses caused by the deformation of the grains and the contribution to the driving force from the elastic energy can be ignored. A 'steady-state' stress distribution is developed in the grain-boundaries and the grains can be considered as rigid. This is one of the basic assumptions of the current model which is valid for problems like long-term creep under low level of stresses, superplastic deformation and free sintering of fine particles, etc.

Under the rigid grain assumption, each grain has only three degrees of freedom to define its motion. Fig. 8 illustrates the grain-boundary diffusion and the associate grain motion. The "centres" of the two grains have been arbitrarily chosen as C_1 at x_{c_1} and y_{c_1}, and C_2 at x_{c_2} and y_{c_2}, where their translational velocities, u_i and v_i, and the rotational velocity, w_i, are defined, in which $i = 1, 2$. The matter redistribution along a grain-boundary results in either a separating or an approaching velocity, referred to as υ_{gb}, between the two grains. υ_{gb} is taken as positive if the grains separate and the direction of υ_{gb} is always normal to the grain-boundary. The separation velocity can be related to the velocities of two rigid grains in the following form:

$$\upsilon_{gb}(\zeta) = [B_1(\zeta)\ B_2(\zeta)\ B_3(\zeta)\ B_4(\zeta)\ B_5(\zeta)\ B_6(\zeta)] \begin{bmatrix} u_1 \\ v_1 \\ w_1 \\ u_2 \\ v_2 \\ w_2 \end{bmatrix}, \tag{35}$$

where

$$\begin{aligned} B_1(\zeta) &= -n_{gb,x}, \\ B_2(\zeta) &= -n_{gb,y}, \\ B_3(\zeta) &= (y(\zeta) - y_{c_1})n_{gb,x} - (x(\zeta) - x_{c_1})n_{gb,y}, \\ B_4(\zeta) &= n_{gb,x}, \\ B_5(\zeta) &= n_{gb,y}, \\ B_6(\zeta) &= -(y(\zeta) - y_{c_2})n_{gb,x} + (x(\zeta) - x_{c_2})n_{gb,y}, \end{aligned}$$

in which, as shown in Fig. 8, $n_{gb,x}$ and $n_{gb,y}$ are the x- and y-components of the normal to the grain-boundary element and $x(\zeta)$ and $y(\zeta)$ are given by Eqs. (10) and (11), respectively.

Matter conservation requires that the separation velocity, υ_{gb}, and the diffusive flux, j_{gb}, along the grain-boundary satisfy the following relationship:

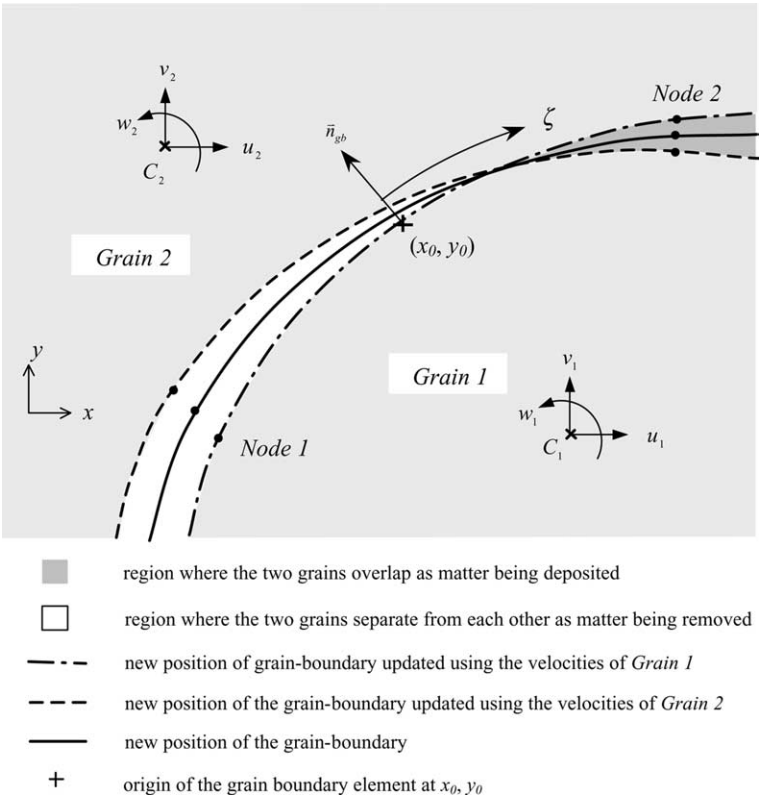

Fig. 8. A grain-boundary diffusion element showing all the degrees of freedom. The dashed lines show that the two grains move relatively to each other as the consequence of matter being removed from the overlapping region to the gap region. A new grain-boundary, shown by the solid line, is placed at the middle of the two dashed lines.

$$v_{\mathrm{gb}} + \frac{\partial j_{\mathrm{gb}}}{\partial S} = 0, \tag{36}$$

in which S is the local coordinate along the grain-boundary. Therefore, we have

$$j_{\mathrm{gb}}(\zeta) = -S_{\mathrm{e}} \int_0^{\zeta} v_{\mathrm{gb}}(\zeta)\,\mathrm{d}\zeta + j_{\mathrm{gb},0}, \tag{37}$$

in which $j_{\mathrm{gb},0}$ is the diffusive flux across the origin of the grain-boundary element. Substituting Eq. (35) into (37) gives

$$j_{\mathrm{gb}}(\zeta) = [H_1(\zeta)\ H_2(\zeta)\ H_3(\zeta)\ H_4(\zeta)\ H_5(\zeta)\ H_6(\zeta)\ 1] \begin{bmatrix} u_1 \\ v_1 \\ w_1 \\ u_2 \\ v_2 \\ w_2 \\ j_{\mathrm{gb},0} \end{bmatrix}, \tag{38}$$

where

$$\left.\begin{aligned} H_1(\zeta) &= -y(\zeta) + y_0, \\ H_2(\zeta) &= x(\zeta) - x_0, \\ H_3(\zeta) &= -\tfrac{1}{2}(y_0 - y(\zeta))(y_0 + y(\zeta) - 2y_{c_1}) \\ &\quad -\tfrac{1}{2}(x_0 - x(\zeta))(x_0 + x(\zeta) - 2x_{c_1}), \\ H_4(\zeta) &= y(\zeta) - y_0, \\ H_5(\zeta) &= -x(\zeta) + x_0, \\ H_6(\zeta) &= \tfrac{1}{2}(y_0 - y(\zeta))(y_0 + y(\zeta) - 2y_{c_2}) \\ &\quad +\tfrac{1}{2}(x_0 - x(\zeta))(x_0 + x(\zeta) - 2x_{c_2}), \end{aligned}\right\} \tag{39}$$

in which x_0 and y_0 are the coordinates of origin of ζ located at the middle of the grain-boundary element. The contribution of the grain-boundary diffusion element to the functional Π^* can be written as:

$$\int_{\Gamma_e} \frac{1}{2M_{gb}} j_{gb}^2 \, d\Gamma = \frac{S_e}{2M_{gb}} \int_{-1}^{1} j_{gb}^2(\zeta) \, d\zeta = \frac{1}{2} [u_1 \ v_1 \ w_1 \ u_2 \ v_2 \ w_2 \ j_{gb,0}][K_{gb}] \begin{bmatrix} u_1 \\ v_1 \\ w_1 \\ u_2 \\ v_2 \\ w_2 \\ j_{gb,0} \end{bmatrix}, \tag{40}$$

in which $[K_{gb}]$ is a 7×7 viscosity matrix for grain-boundary diffusion. Its detailed form is provided in Appendix A.

Similar to free surface diffusion, a Lagrange multiplier, λ_{gb} is introduced at each node to enforce the continuity of grain-boundary flux because it is not guaranteed by expression (38). The contribution of the Lagrange terms from each grain-boundary element to the functional Π^* is then

$$\frac{1}{2} [\lambda_{gb,2} \ \lambda_{gb,1}] \begin{bmatrix} j_{gb}(1) \\ -j_{gb}(-1) \end{bmatrix} = \frac{1}{2} [\lambda_{gb,2} \ \lambda_{gb,1}][C_{gb}] \begin{bmatrix} u_1 \\ v_1 \\ w_1 \\ u_2 \\ v_2 \\ w_2 \\ j_{gb,0} \end{bmatrix}, \tag{41}$$

where $[C_{gb}]$ is a 2×7 complimentary matrix and provided in Appendix A. Eqs. (40) and (41) can be combined into the following:

$$\frac{1}{2} [u_1 \ v_1 \ w_1 \ u_2 \ v_2 \ w_2 \ j_{gb,0} \ \lambda_{gb,2} \ \lambda_{gb,1}] \begin{bmatrix} [K_{gb}] & [C_{gb}]^T \\ [C_{gb}] & 0 \end{bmatrix} \begin{bmatrix} u_1 \\ v_1 \\ w_1 \\ u_2 \\ v_2 \\ w_2 \\ j_{gb,0} \\ \lambda_{gb,2} \\ \lambda_{gb,1} \end{bmatrix} = \frac{1}{2} [U_{gb}]^T [A_{gb}][U_{gb}], \tag{42}$$

in which $[U_{gb}]$ is the vector of elementary unknowns and $[A_{gb}]$ is the generalised viscosity matrix for the grain-boundary diffusion element. Where a grain-boundary meets either a free surface or other grain-boundaries, matter conservation is guaranteed by the corresponding Lagrange term in the variational principle.

7. Coupling, global equations and time integration

In the above sections, the functional Π^* has been discretised for surface diffusion, grain-boundary migration and grain-boundary diffusion, respectively. The three processes are strongly coupled. The grain-boundary diffusion and surface diffusion are connected at all the junctions between the grain-boundary network and free surfaces. The grain-boundary diffusion occurs as the boundaries migrate, and the grain-boundary migration and surface migration share a common velocity where a grain-boundary meets a free surface. All these coupling conditions are included in the variational principle. The balance of the interfacial tensions at any triple junction, which defines the angle at which the interfaces meet each other (the dihedral angle), is also guaranteed by the variational principle. Therefore, the finite element solution for the velocity of a triple junction and the velocities of the grain-boundaries and free surface in the vicinity of the triple junction are such that the correct dihedral angle is maintained at each timestep. Furthermore, at a junction between a grain-boundary and a free surface, there is an exchange of free energy as the grains move relative to each other and the junction is relocated. This leads to an extra contribution to the force term. A detailed treatment of the triple junction relating to the above issues has been provided by Pan et al. [18] which does not depend on the type of the finite element and is not repeated here.

Collecting all the contributions together provides a discretised expression of Π^* in terms of all the degrees of freedom shown in Fig. 1:

$$\Pi^* = \frac{1}{2}[U]^{\mathrm{T}}[A][U] + [F][U], \tag{43}$$

where $[U]$ is the vector of global unknowns, which consists of $[U_s]$, $[U_m]$ and $[U_{gb}]$. It contains the velocities of individual grains (two translational and one rotational for each grain), nodal migration velocities of grain-boundaries and free surfaces, diffusive fluxes across the mid-points of surface and grain-boundary diffusion elements, and Lagrange multipliers at every node. $[A]$ is the generalised global viscosity matrix which is assembled from $[A_s]$, $[A_m]$ and $[A_{gb}]$. $[F]$ is the global force vector which is assembled from $[F_s]$, $[F_m]$ and $[F_{gb}]$. The variational principle requires that $\delta\Pi^* = 0$, which leads to

$$[A][U] + [F] = 0. \tag{44}$$

The above equations can be solved using a standard numerical solver.

The position of the entire network of grain-boundaries and free surfaces can then be updated using a time integration scheme, the direct Euler method, for example. The updating procedure has been discussed in detail in the previous papers by Pan, Cocks, and their co-workers [16–18]. All the procedures used previously are valid here except for how to update the position of the grain-boundaries. The new position of a grain-boundary is determined from the superposition of the contributions from the grain-boundary migration and grain-boundary diffusion, respectively. At each timestep, the grain-boundary position is first updated using the grain-boundary migration velocity which is straightforward. Subsequently the grain-boundary position is updated again from the rigid motion of the grains (the order of these two updating steps does not actually matter and can be swapped). As shown in Fig. 8, the new position of the grain-boundary as the consequence of the matter redistribution (grain-boundary diffusion) should be between the imaginary positions, illustrated using the two dashed lines, of the two grain-boundaries updated using the velocities of the two grains. The actual position of the "new" grain-boundary should be such that it minimises the total free energy within the constraint. Such a minimisation is, however, too complicated and we simply average the positions of two updated boundaries to obtain a "new" cubic spline position for the grain-boundary. At any triple junction, the "new" position of the triple junction is relocated at the average positions of the three intersecting points between the three interfaces as shown in Fig. 9. These procedures inevitably introduce small errors; however, any significant updating error is automatically corrected by the finite element solution in the next timestep.

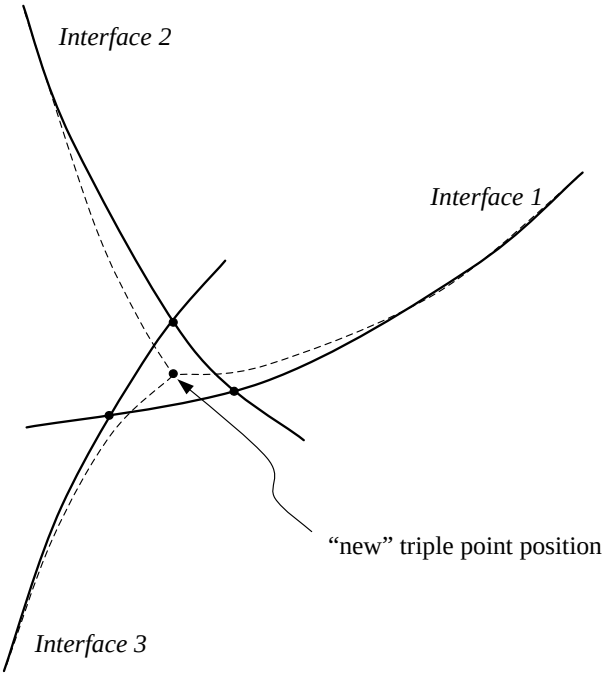

Fig. 9. Updating the triple junction. The three interfaces do not usually meet at one location after their positions are updated. The problem is overcome by relocating the triple junction at the average position of the three joints between the three interfaces.

8. Numerical examples

In this section, we present several numerical examples for which analytical solutions can be obtained. The finite element formulations are first verified against the analytical solutions for surface diffusion, grain-boundary migration and grain-boundary diffusion separately, and then against analytical solutions for the coupled cases. Finally the finite element scheme is used to simulate numerically the co-sintering process of two cylindrical particles of different sizes which involves all the three kinetic processes.

8.1. Surface diffusion

An isolated elliptical cavity in a solid material can evolve toward a circular one by surface diffusion in order to reduce its total surface area. At $t = 0$, analytical expressions for the surface diffusion flux, surface migration velocity and Lagrange multiplier for the flux continuity can be obtained [18]. These analytical solutions can be used to verify the cubic spline finite element formulation for surface diffusion presented in Section 4. Fig. 10 shows the comparison between the finite element solutions and the analytical expressions. Seven cubic spline elements are used for a quarter of the cavity. It can be seen that the finite element solutions agree very well with the analytical expressions. Fig. 11 compares the finite element solution with a finite difference solution for the temporal evolution of the cavity surface. In the finite difference solution (solid lines), 100 nodes are used along a quarter of the cavity surface. In the finite element solution (discrete dots), only three elements are used. It can be seen that the finite element formulation for surface diffusion works very well.

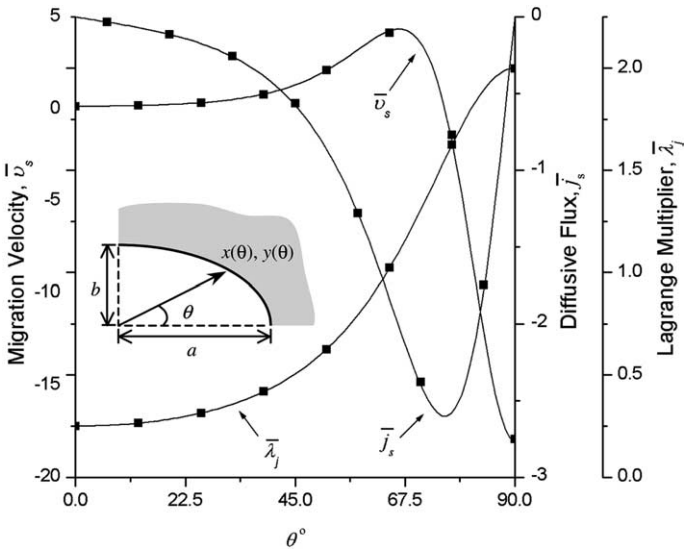

Fig. 10. Comparison between the numerical and analytical solutions for the surface migration velocity, υ_s diffusive flux, j_s and Lagrange multiplier, λ_j for the problem of diffusion along the free surface of an elliptical cavity. Seven cubic spline elements are used to model a quarter of the cavity. In this example, $a/b = 2$, $M_s = 1$ and $\gamma_s = 1$. The analytical and numerical solutions are represented by solid lines and square boxes, respectively.

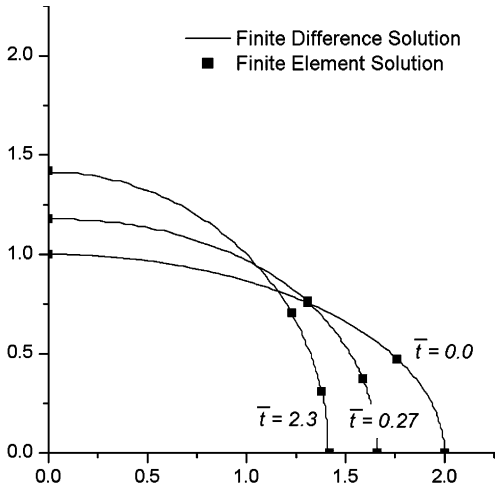

Fig. 11. Comparison between the finite element and finite difference solutions for the temporal evolution of the elliptical cavity.

8.2. Grain-boundary migration

A circular grain embedded in a larger grain of identical material shrinks until it disappears with the velocity:

$$\frac{\mathrm{d}R}{\mathrm{d}t} = -M_{\mathrm{m}}\gamma_{\mathrm{gb}}\frac{1}{R}, \tag{45}$$

in which R is the radius of the circular grain, M_m, the grain-boundary migration mobility and γ_{gb}, the specific grain-boundary energy. This equation can be integrated to verify the cubic spline element for grain-boundary migration presented in Section 5. Due to symmetry, we model a quarter of the circular grain using three cubic spline elements. Fig. 12 presents the comparison between the finite element solution and the analytical solution for the temporal evolution of the circular grain at two different times. It can be seen that the two solutions agree very well.

8.3. Grain-boundary diffusion

The cubic spline element formulation for grain-boundary diffusion is verified using two numerical examples here. First, we consider a semi-circular grain-boundary as shown in Fig. 13. The two grains are subjected to a remote force, F and the separation velocity between the two grains is referred to as u_∞. We further impose the boundary conditions that the capillarity stress is zero where the grain-boundary meets the two surfaces and that the diffusive flux, j_{gb} is zero across the symmetry point ($\theta = 0^\circ$). The problem can be solved analytically providing the following expressions for u_∞, j_{gb} and the stress, σ, normal to the grain-boundary:

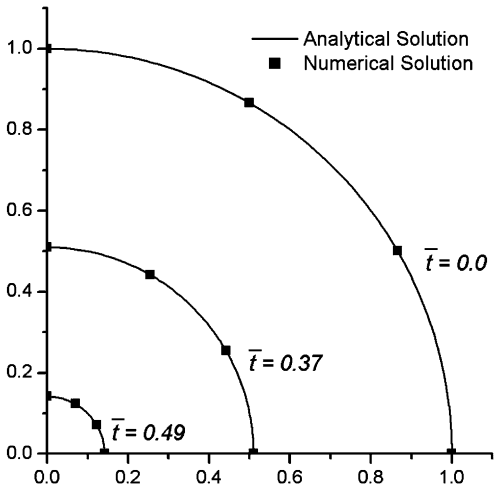

Fig. 12. Comparison between the finite element and analytical solutions for the boundary migration of a circular grain which is embedded in a bigger grain of identical material.

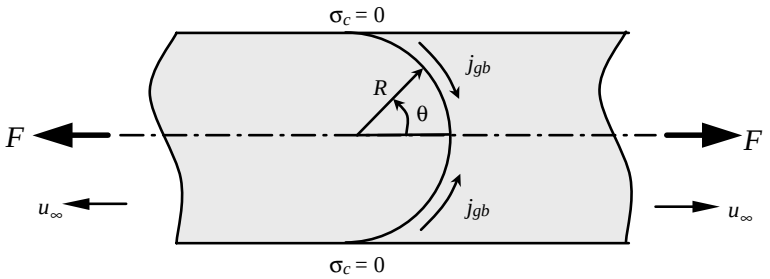

Fig. 13. A semi-circular grain-boundary between two grains is subjected to a remote force F leading to a remote separation velocity of u_∞ between the two grains.

$$u_\infty = \frac{2M_{\mathrm{gb}}}{\pi R^3} F, \tag{46}$$

$$j_{\mathrm{gb}} = -u_\infty R \sin\theta \tag{47}$$

and

$$\sigma = \frac{u_\infty R^2 \cos\theta}{M_{\mathrm{gb}}}. \tag{48}$$

The same problem is solved using five equally spaced cubic spline elements presented in Section 6. No time integration is undertaken because our purpose here is to verify the finite element formulation not the time integration scheme. We use several sets of arbitrary input data in the numerical analysis. The finite element solution agrees very well with the analytical solution for all the input data. For example, when using $M_{\mathrm{gb}} = 18$, $R = 1$ and $F = 9573$, the finite element solution for u_∞ was 1.09754×10^5 while Eq. (46) predicts $u_\infty = 1.09698 \times 10^5$. Fig. 14 compares the finite element solution with Eqs. (47) and (48). It can be seen that the two solutions agree very well with each other.

To verify the cubic spline element when the grains rotate, we consider a straight grain-boundary which is subjected to a bending moment, M_∞, producing a relative angular velocity, ω_∞, between the two grains as shown in Fig. 15. We further impose the boundary condition that the capillarity stress where the grain-boundary meets the two surfaces is zero. A straightforward analytical solution to this problem is obtained and then the same problem is solved using five equally space cubic spline elements. Again a few sets of arbitrary data of the material and geometry parameters are used in the test. In all the cases, the two solutions agree with each other very well. For example, for $M_\infty = 55,382$, $M_{\mathrm{gb}} = 23.5$ and $L = 1$, the analytical solution gives $\omega_\infty = 2.9283 \times 10^7$ which can be compared to the finite element solution of $\omega_\infty = 2.9283 \times 10^7$. Fig. 16 presents the comparison of the two solutions for the diffusive flux and the grain-boundary stress. The two solutions agree very well with each other.

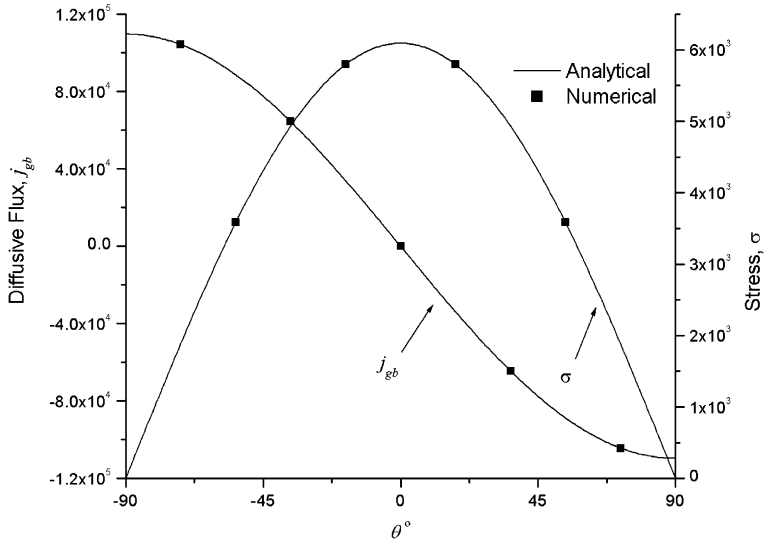

Fig. 14. Comparison between the analytical and numerical solutions for the grain-boundary stress, σ, and the diffusive flux, j_{gb} for the semi-circular grain-boundary shown in Fig. 13.

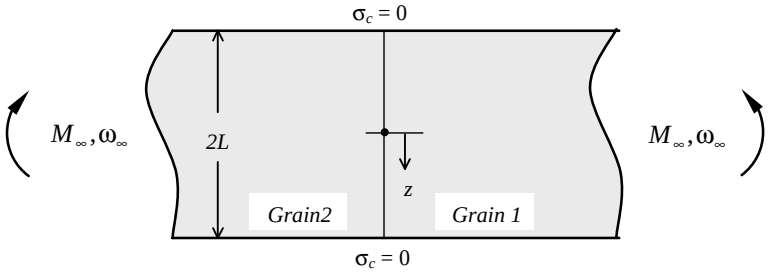

Fig. 15. A straight grain-boundary between two grains is subjected to a bending moment M_∞ leading to a relative rational velocity ω_∞ between the two grains.

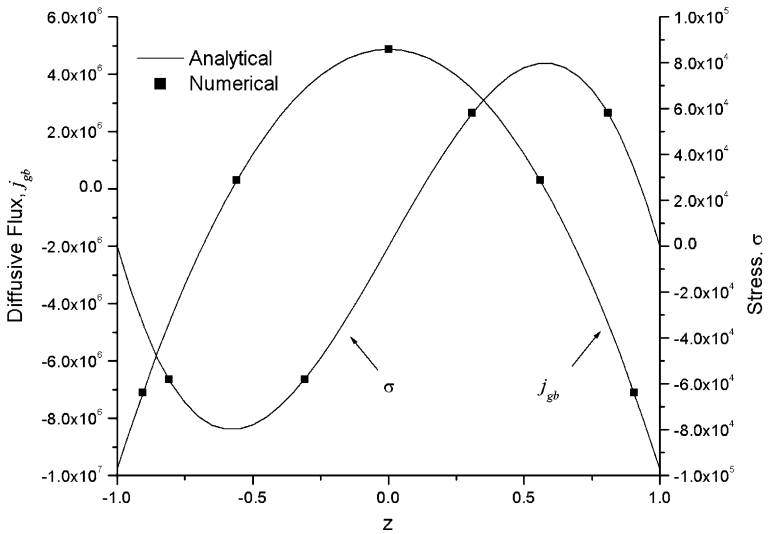

Fig. 16. Comparison between the analytical and numerical solutions for the grain-boundary stress, σ, and the diffusive flux, j_{gb}, for the straight grain-boundary shown in Fig. 15.

8.4. Coupled grain-boundary migration and surface diffusion

To verify the special elements for surface diffusion and grain-boundary migration, we consider a case of thermal grooving at a migrating grain-boundary as shown in Fig. 17. Two infinitively long grains sit on a single crystal substrate. The interface between the right grain and the substrate is assigned a higher specific

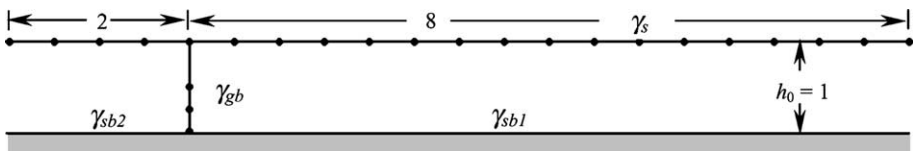

Fig. 17. Thermal grooving at a migrating grain-boundary – the initial geometry of a film of two grains, which sit on a substrate. The initial finite element nodes are shown using the discrete symbols.

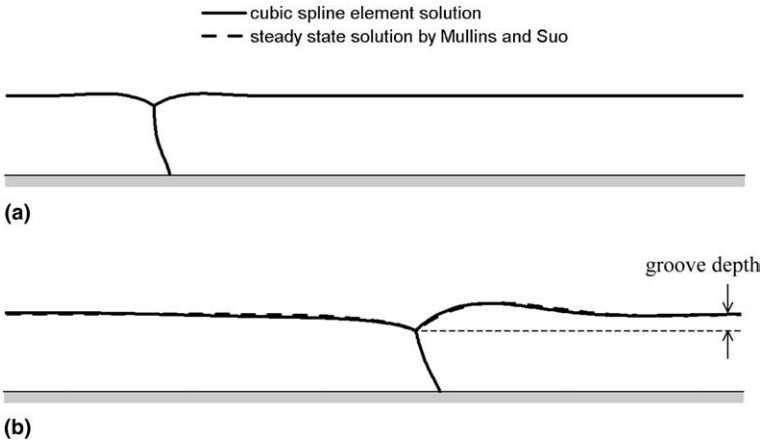

Fig. 18. Finite element simulation of the boundary migration in the film and thermal grooving at the top triple junction. In (b) the finite element solution (solid lines) at $\bar{t} = 0.6045$ is compared to the analytical solution (dashed lines) at the steady state which were obtained by Mullins [12] and Suo [22].

energy than that between the left grain and the substrate, i.e., $\gamma_{sb_1} > \gamma_{sb_2}$. The vertical grain-boundary migrates to the right to reduce the total free energy of the system. At the same time, the junction between the grain-boundary and the top surface grooves by surface diffusion.

Mullins [12] and Suo [22] obtained a set of steady-state solutions for this problem. Pan et al. [18] used their analytical solutions to verify their linear elements. Here, we use the same analytical solutions to verify the cubic spline elements. The finite element mesh at $\bar{t} = 0$ is shown in Fig. 17 using the discrete symbols. As the grain-boundary migrates to the right, frequent re-meshing has to be undertaken to continue the numerical simulation. The numerical integration is carried out until a steady state is reached where it can be compared to the analytical solutions. Again a few set of arbitrary input data of the material parameters are used, and for all the cases the results from the analytical and finite element solutions agree with each other well at the steady state. Fig. 18 presents the finite element solutions for $\gamma_{gb}/\gamma_s = 1$, $\gamma_{sb_1}/\gamma_s = 1.5$, $\gamma_{sb_2}/\gamma_s = 1$, $M_m h_0^2/M_s = 10.4$. Fig. 18(a) shows the numerical solution before the steady state is reached. Fig. 18(b) compares the finite element solution (dashed lines) with the analytical solutions (solid lines) at the steady state. Furthermore, the groove depth at the steady state, as defined in Fig. 18(b), is predicted as 0.204, 0.196 and 0.166 by the steady-state analytical solution [12], the cubic spline elements and the linear elements [18], respectively.

8.5. Coupled grain-boundary and surface diffusion

To verify the Lagrange terms introduced in the variational principle which enforce the coupling conditions between surface diffusion and grain-boundary diffusion, we consider a case of cavity growth at the triple grain-boundary junctions in a hexagonal polycrystalline structure as shown in Fig. 19(a). Cocks and Searle [7] obtained an analytical solution for the remote strain rates $\dot{\varepsilon}_1^\infty$ and $\dot{\varepsilon}_2^\infty$ at the extreme of fast surface diffusion. Here, we use the cubic spline elements for a representative unit of the problem as shown by the dashed line in Fig. 19(a) which is enlarged in Fig. 19(b) and calculate the remote strain rates for a range of material parameters. The finite element nodes used in the model can also be clearly seen in Fig. 19(b). Fig. 20 presents the finite element solution for $\dot{\varepsilon}_1^\infty$ as a function of the ratio between the surface diffusivity over the grain-boundary diffusivity. The other parameters used in the numerical solution were $\sigma_1 = 0$, $\sigma_2 = 0$, $\gamma_s = 1$, $\gamma_{gb} = 0$, $R = 30$ and grain size, $d = 346.4102$. From the figure, it can be seen that the finite element solution approaches the equilibrium growth solution for fast surface diffusion as $M_s/M_{gb} \geqslant 4$. At the extreme of fast surface diffusion, i.e., for $M_s \gg M_{gb}$, the finite element solution agrees well with Cocks

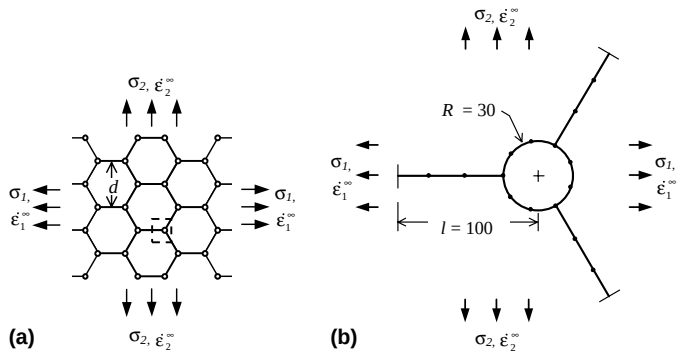

Fig. 19. Cavity growth at triple grain-boundary junctions in a hexagonal polycrystalline structure. (b) The representative unit and the nodal positions used in the finite element model.

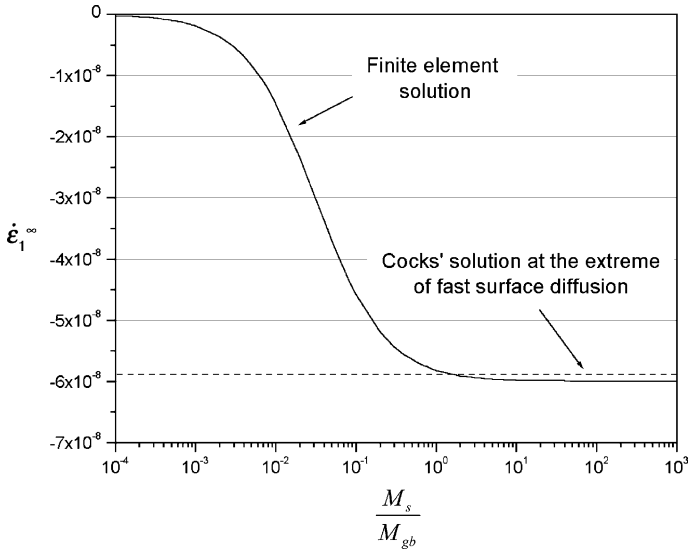

Fig. 20. Finite element solution of the remote strain rate in the horizontal direction for the problem shown in Fig. 19 as a function of M_s/M_{gb}. No stress is applied hence the cavity sinters under the capillarity stress leading to the shrinkage of the material. The dashed line is the analytical solution obtained by Cocks and Searle [7] who assumed fast surface diffusion, i.e., $M_s \gg M_{gb}$.

and Searle's analytical solution [7]. It is interesting to notice that the analytical solution assuming equilibrium growth works surprisingly well.

8.6. Co-sintering of two cylindrical particles of different sizes

To demonstrate the finite element scheme for a fully coupling process between grain-boundary diffusion, surface diffusion and grain-boundary migration, we consider the co-sintering process of two cylindrical particles of two different sizes as shown in Fig. 21(a). At elevated temperatures atoms are transported from the contact neck between the two particles to the triple junction through grain-boundary diffusion and taken away from the junction and deposited onto the free surfaces through surface diffusion. This process is accompanied by the migration of the neck (grain-boundary) towards the smaller particle leading to grain-growth. Pan, Cocks and their co-workers [17,20] were the first to study this problem using a numerical method. Zhang et al. [25] also

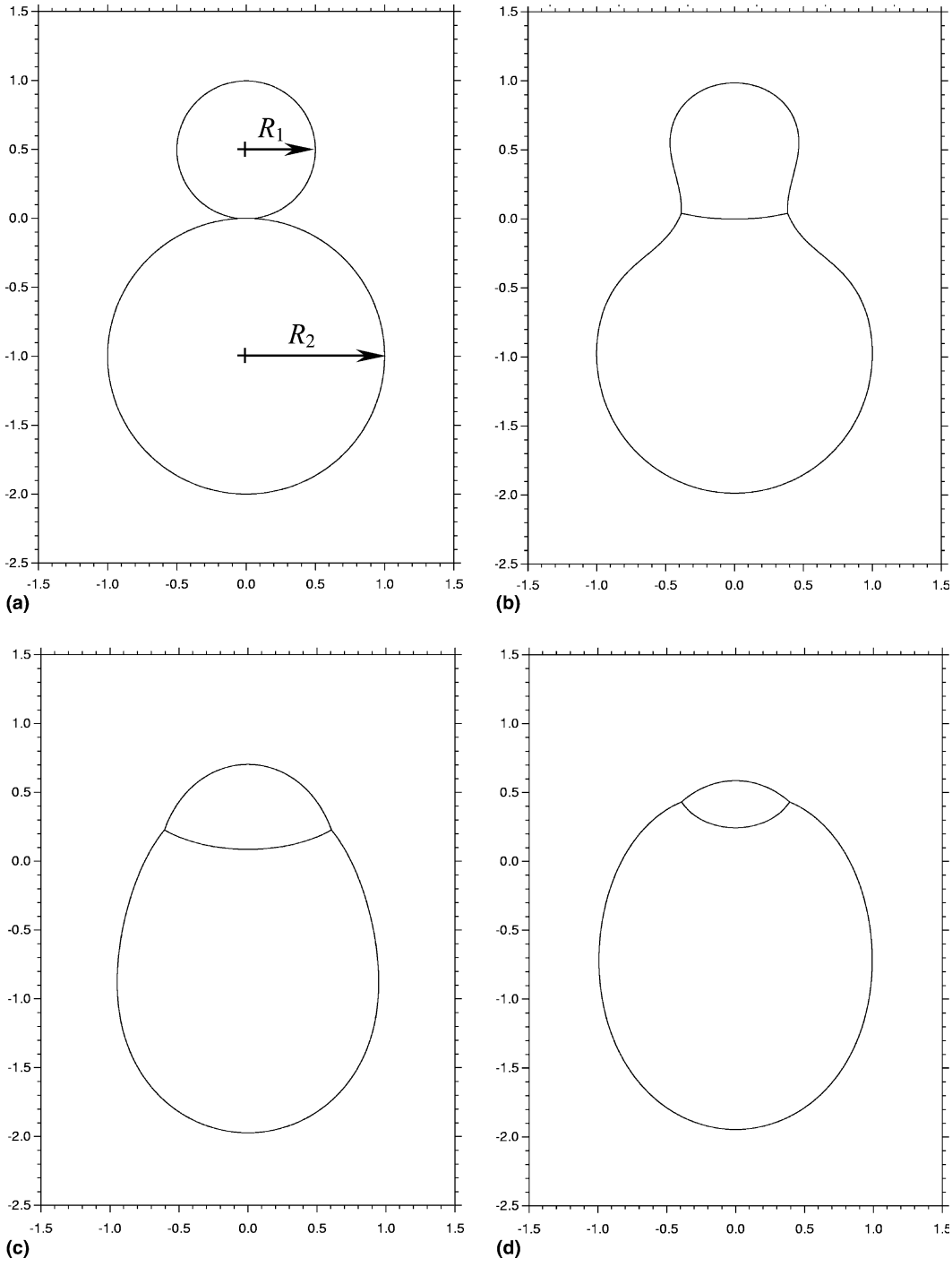

Fig. 21. Computer simulated co-sintering process of two cylindrical particles of different sizes. All the three kinetic processes, i.e., grain-boundary diffusion, surface diffusion and grain-boundary migration, are modelled. (a) $\bar{t}_0 = 0.0$, (b) $\bar{t}_1 = 3.423 \times 10^{-5}$, (c) $\bar{t}_2 = 1.558 \times 10^{-3}$ and (d) $\bar{t}_3 = 3.109 \times 10^{-3}$. The ratio of the initial radii is $R_1/R_2 = 0.5$. $M_s/M_{gb} = 10$, $M_m R_2^2/M_{gb} = 100$, $\gamma_s/\gamma_{gb} = 3$.

undertook detailed numerical studies of the same problem. However, Pan et al. assumed fast grain-boundary migration in their model and Zhang et al. did not consider grain-boundary diffusion in their model. Using the finite element scheme developed in this paper, we can for the first time consider the full coupling between all the three kinetic processes. Figs. 21(b)–(d) present the numerical simulation of the co-sintering process. The following parameters were used in this example: $R_1/R_2 = 0.5, \gamma_s/\gamma_{gb} = 3, M_s/M_{gb} = 10$ and $M_m R_2^2/M_{gb} = 100$. An important observation from these figures is that the time taken by the neck to become approximately equal to the size of the smaller particle (at time $\bar{t}_1$ shown in Fig. 21(b)) is a very tiny fraction of the entire co-sintering process. This shows that the neck growth and grain-growth are almost two consecutive processes in the sintering process. A large number of similar computer simulations have been carried out covering a wide range of material parameters, which will be published in a forthcoming paper.

9. Concluding remarks

The cubic spline finite element formulations enforce the smoothness of the interface to the continuity of second derivatives. Such a numerical approach filters out the high frequency oscillation of the interface during their migration and focuses the numerical solution on the global evolution of the microstructure. The numerical scheme has made it possible to model each interface using as little as three finite elements in a complicated microstructure. This numerical advantage is fully exploited in a separate paper in which the finite element scheme is used to investigate the sintering behaviour of large pores in particle compact [19]. There the numerical tool helped us to gain a deep insight into the material behaviour and some of the classical textbook theory for sintering was shown to be inappropriate.

Acknowledgements

H.N. Ch'ng gratefully acknowledges a PhD studentship from the University of Surrey.

Appendix A. Generalised viscosity matrixes for surface diffusion, grain-boundary migration and grain-boundary diffusion

A.1. Generalised viscosity matrixes for surface diffusion

$$[K_s] = \begin{bmatrix} \frac{23}{120}\frac{S_e^3}{M_s} & \frac{17}{120}\frac{S_e^3}{M_s} & -\frac{4}{15}\frac{S_e^5}{M_s} & -\frac{17}{21}\frac{S_e^6}{M_s} & \frac{1}{6}\frac{S_e^2}{M_s} \\ & \frac{23}{120}\frac{S_e^3}{M_s} & -\frac{4}{15}\frac{S_e^5}{M_s} & -\frac{83}{105}\frac{S_e^6}{M_s} & -\frac{1}{6}\frac{S_e^2}{M_s} \\ & & \frac{136}{315}\frac{S_e^7}{M_s} & \frac{136}{105}\frac{S_e^8}{M_s} & 0 \\ & \text{Symmetric} & & \frac{248}{63}\frac{S_e^9}{M_s} & -\frac{4}{15}\frac{S_e^5}{M_s} \\ & & & & 2\frac{S_e}{M_s} \end{bmatrix},$$

$$[C_s] = \begin{bmatrix} -\frac{1}{2S_e} & \frac{1}{2S_e} & 2S_e & 8S_e^2 & 0 \\ \frac{1}{2S_e} & -\frac{1}{2S_e} & 2S_e & 4S_e^2 & 0 \\ 0 & 0 & 2 & 12S_e & 0 \\ 0 & 0 & -2 & 0 & 0 \\ -\frac{1}{4}S_e & -\frac{3}{4}S_e & \frac{2}{3}S_e^3 & 2S_e^4 & 1 \\ -\frac{3}{4}S_e & -\frac{1}{4}S_e & \frac{2}{3}S_e^3 & 2S_e^4 & -1 \end{bmatrix}.$$

A.2. Generalised viscosity matrixes for special element of surface diffusion

$$\left[K_{\mathrm{s}}^{*}\right]=\begin{bmatrix}
\frac{23}{120}\frac{S_{\mathrm{e}}^{3}n_x^{2}}{M_{\mathrm{s}}} & \frac{23}{120}\frac{S_{\mathrm{e}}^{3}n_xn_y}{M_{\mathrm{s}}} & \frac{17}{120}\frac{S_{\mathrm{e}}^{3}n_x}{M_{\mathrm{s}}} & -\frac{4}{15}\frac{S_{\mathrm{e}}^{5}n_x}{M_{\mathrm{s}}} & -\frac{17}{21}\frac{S_{\mathrm{e}}^{6}n_x}{M_{\mathrm{s}}} & \frac{1}{6}\frac{S_{\mathrm{e}}^{2}n_x}{M_{\mathrm{s}}}\\
 & \frac{23}{120}\frac{S_{\mathrm{e}}^{3}n_y^{2}}{M_{\mathrm{s}}} & \frac{17}{120}\frac{S_{\mathrm{e}}^{3}n_y}{M_{\mathrm{s}}} & -\frac{4}{15}\frac{S_{\mathrm{e}}^{5}n_y}{M_{\mathrm{s}}} & \frac{17}{21}\frac{S_{\mathrm{e}}^{6}n_y}{M_{\mathrm{s}}} & \frac{1}{6}\frac{S_{\mathrm{e}}^{2}n_y}{M_{\mathrm{s}}}\\
 & & \frac{23}{120}\frac{S_{\mathrm{e}}^{3}}{M_{\mathrm{s}}} & -\frac{4}{15}\frac{S_{\mathrm{e}}^{5}}{M_{\mathrm{s}}} & -\frac{83}{105}\frac{S_{\mathrm{e}}^{6}}{M_{\mathrm{s}}} & -\frac{1}{6}\frac{S_{\mathrm{e}}^{2}}{M_{\mathrm{s}}}\\
 & & & \frac{136}{315}\frac{S_{\mathrm{e}}^{7}}{M_{\mathrm{s}}} & \frac{136}{105}\frac{S_{\mathrm{e}}^{8}}{M_{\mathrm{s}}} & 0\\
 & \text{Symmetric} & & & \frac{248}{63}\frac{S_{\mathrm{e}}^{9}}{M_{\mathrm{s}}} & -\frac{4}{15}\frac{S_{\mathrm{e}}^{5}}{M_{\mathrm{s}}}\\
 & & & & & 2\frac{S_{\mathrm{e}}}{M_{\mathrm{s}}}
\end{bmatrix},$$

$$\left[C_{\mathrm{s}}^{*}\right]=\begin{bmatrix}
-\frac{n_x}{2S_{\mathrm{e}}} & -\frac{n_y}{2S_{\mathrm{e}}} & \frac{1}{2S_{\mathrm{e}}} & 2S_{\mathrm{e}} & 8S_{\mathrm{e}}^{2} & 0\\
0 & 0 & 0 & 2 & 12S_{\mathrm{e}} & 0\\
-\frac{1}{4}n_xS_{\mathrm{e}} & -\frac{1}{4}n_yS_{\mathrm{e}} & -\frac{3}{4}S_{\mathrm{e}} & \frac{2}{3}S_{\mathrm{e}}^{3} & 2S_{\mathrm{e}}^{4} & 1\\
-\frac{3}{4}n_xS_{\mathrm{e}} & -\frac{3}{4}n_yS_{\mathrm{e}} & -\frac{1}{4}S_{\mathrm{e}} & \frac{2}{3}S_{\mathrm{e}}^{3} & 2S_{\mathrm{e}}^{4} & -1
\end{bmatrix}.$$

A.3. Generalised viscosity matrixes for grain-boundary migration

$$\left[K_{\mathrm{m}}\right]=\begin{bmatrix}
\frac{2}{3}\frac{S_{\mathrm{e}}}{M_{\mathrm{m}}} & \frac{1}{3}\frac{S_{\mathrm{e}}}{M_{\mathrm{m}}} & -\frac{2}{3}\frac{S_{\mathrm{e}}^{3}}{M_{\mathrm{m}}} & -\frac{28}{15}\frac{S_{\mathrm{e}}^{4}}{M_{\mathrm{m}}}\\
 & \frac{2}{3}\frac{S_{\mathrm{e}}}{M_{\mathrm{m}}} & -\frac{2}{3}\frac{S_{\mathrm{e}}^{3}}{M_{\mathrm{m}}} & -\frac{32}{15}\frac{S_{\mathrm{e}}^{4}}{M_{\mathrm{m}}}\\
 & & \frac{16}{15}\frac{S_{\mathrm{e}}^{5}}{M_{\mathrm{m}}} & \frac{16}{5}\frac{S_{\mathrm{e}}^{6}}{M_{\mathrm{m}}}\\
 & \text{Symmetric} & & \frac{1024}{105}\frac{S_{\mathrm{e}}^{7}}{M_{\mathrm{m}}}
\end{bmatrix},$$

$$\left[C_{\mathrm{m}}\right]=\begin{bmatrix}
-\frac{1}{2S_{\mathrm{e}}} & \frac{1}{2S_{\mathrm{e}}} & 2S_{\mathrm{e}} & 8S_{\mathrm{e}}^{2}\\
\frac{1}{2S_{\mathrm{e}}} & -\frac{1}{2S_{\mathrm{e}}} & 2S_{\mathrm{e}} & 4S_{\mathrm{e}}^{2}\\
0 & 0 & 2 & 12S_{\mathrm{e}}\\
0 & 0 & -2 & 0
\end{bmatrix}.$$

A.4. Generalised viscosity matrixes for special element of grain-boundary migration

$$\left[K_{\mathrm{m}}^{*}\right]=\begin{bmatrix}
\frac{2}{3}\frac{S_{\mathrm{e}}}{M_{\mathrm{m}}} & \frac{1}{3}\frac{S_{\mathrm{e}}n_x}{M_{\mathrm{m}}} & \frac{1}{3}\frac{S_{\mathrm{e}}n_y}{M_{\mathrm{m}}} & -\frac{2}{3}\frac{S_{\mathrm{e}}^{3}}{M_{\mathrm{m}}} & -\frac{28}{15}\frac{S_{\mathrm{e}}^{4}}{M_{\mathrm{m}}}\\
 & \frac{2}{3}\frac{S_{\mathrm{e}}n_x^{2}}{M_{\mathrm{m}}} & \frac{2}{3}\frac{S_{\mathrm{e}}n_xn_y}{M_{\mathrm{m}}} & -\frac{2}{3}\frac{S_{\mathrm{e}}^{3}n_x}{M_{\mathrm{m}}} & -\frac{32}{15}\frac{S_{\mathrm{e}}^{4}n_x}{M_{\mathrm{m}}}\\
 & & \frac{2}{3}\frac{S_{\mathrm{e}}n_y^{2}}{M_{\mathrm{m}}} & -\frac{2}{3}\frac{S_{\mathrm{e}}^{3}n_y}{M_{\mathrm{m}}} & -\frac{32}{15}\frac{S_{\mathrm{e}}^{4}}{M_{\mathrm{m}}}\\
 & \text{Symmetric} & & \frac{16}{15}\frac{S_{\mathrm{e}}^{5}}{M_{\mathrm{m}}} & \frac{16}{5}\frac{S_{\mathrm{e}}^{6}}{M_{\mathrm{m}}}\\
 & & & & \frac{1024}{105}\frac{S_{\mathrm{e}}^{7}}{M_{\mathrm{m}}}
\end{bmatrix},$$

$$\left[C_{\mathrm{m}}^{*}\right]=\begin{bmatrix}
\frac{1}{2S_{\mathrm{e}}} & -\frac{n_x}{2S_{\mathrm{e}}} & -\frac{n_y}{2S_{\mathrm{e}}} & 2S_{\mathrm{e}} & 4S_{\mathrm{e}}^{2}\\
0 & 0 & 0 & -2 & 0
\end{bmatrix}.$$

A.5. Generalised viscosity matrixes for grain-boundary diffusion

$$[K_{\mathrm{gb}}] = \frac{S_{\mathrm{e}}}{M_{\mathrm{gb}}} \int_{-1}^{1} \begin{bmatrix} H_1H_1 & H_1H_2 & H_1H_3 & H_1H_4 & H_1H_5 & H_1H_6 & H_1 \\ & H_2H_2 & H_2H_3 & H_2H_4 & H_2H_5 & H_2H_6 & H_2 \\ & & H_3H_3 & H_3H_4 & H_3H_5 & H_3H_6 & H_3 \\ & & & H_4H_4 & H_4H_5 & H_4H_6 & H_4 \\ & & & & H_5H_5 & H_5H_6 & H_5 \\ & \text{Symmetric} & & & & H_6H_6 & H_6 \\ & & & & & & 1 \end{bmatrix} \mathrm{d}\zeta,$$

in which

$$\begin{aligned} H_1(\zeta) &= -y(\zeta) + y_0, \\ H_2(\zeta) &= x(\zeta) - x_0, \\ H_3(\zeta) &= -\tfrac{1}{2}(y_0 - y(\zeta))(y_0 + y(\zeta) - 2y_{c_1}) - \tfrac{1}{2}(x_0 - x(\zeta))(x_0 + x(\zeta) - 2x_{c_1}), \\ H_4(\zeta) &= y(\zeta) - y_0, \\ H_5(\zeta) &= -x(\zeta) + x_0, \\ H_6(\zeta) &= \tfrac{1}{2}(y_0 - y(\zeta))(y_0 + y(\zeta) - 2y_{c_2}) + \tfrac{1}{2}(x_0 - x(\zeta))(x_0 + x(\zeta) - 2x_{c_2}). \end{aligned}$$

Gauss quadrature integration can be used to obtain the actual viscosity matrix

$$[C_{\mathrm{gb}}] = \begin{bmatrix} H_1(1) & H_2(1) & H_3(1) & H_4(1) & H_5(1) & H_6(1) & 1 \\ -H_1(-1) & -H_2(-1) & -H_3(-1) & -H_4(-1) & -H_5(-1) & -H_6(-1) & -1 \end{bmatrix},$$

in which

$$\begin{aligned} H_1(1) &= -y_{p_2} + y_0, \\ H_2(1) &= x_{p_2} - x_0, \\ H_3(1) &= -\tfrac{1}{2}(y_0 - y_{p_2})(y_0 + y_{p_2} - 2y_{c_1}) - \tfrac{1}{2}(x_0 - x_{p_2})(x_0 + x_{p_2} - 2x_{c_1}), \\ H_4(1) &= y_{p_2} - y_0, \\ H_5(1) &= -x_{p_2} + x_0, \\ H_6(1) &= \tfrac{1}{2}(y_0 - y_{p_2})(y_0 + y_{p_2} - 2y_{c_2}) + \tfrac{1}{2}(x_0 - x_{p_2})(x_0 + x_{p_2} - 2x_{c_2}), \end{aligned}$$

$$\begin{aligned} H_1(-1) &= -y_{p_1} + y_0, \\ H_2(-1) &= x_{p_1} + x_0, \\ H_3(-1) &= -\tfrac{1}{2}(y_0 - y_{p_1})(y_0 + y_{p_1} - 2y_{c_1}) - \tfrac{1}{2}(x_0 - x_{p_1})(x_0 + x_{p_1} - 2x_{c_1}), \\ H_4(-1) &= y_{p_1} - y_0, \\ H_5(-1) &= -x_{p_1} + x_0, \\ H_6(-1) &= \tfrac{1}{2}(y_0 - y_{p_1})(y_0 + y_{p_1} - 2y_{c_2}) + \tfrac{1}{2}(x_0 - x_{p_1})(x_0 + x_{p_1} - 2x_{c_2}), \end{aligned}$$

where x_{p_1}, y_{p_1} and x_{p_2}, y_{p_2} denote the coordinates of *Node 1* and *Node 2*, respectively, as illustrated in Fig. 8.

References

[1] E. Bänsch, P. Morin, R.H. Nochetto, Finite element methods for surface diffusion, in: Proceedings of Free Boundary Problems: Theory and Applications, Trento, 2002 (to appear).

[2] J.W. Cahn, J.E. Taylor, Surface motion by surface diffusion, Acta Metall. 42 (1994) 1045–1063.
[3] A.C.F. Cocks, A finite element description of grain-boundary diffusion controlled processes in ceramic materials, in: I.M. Allison, C. Ruiz (Eds.), Applied Solid Mechanics, vol. 3, Elsevier, North-Holland, Amsterdam, 1989, pp. 30–42.
[4] A.C.F. Cocks, Variational principles, numerical schemes and bounding theorems for deformation by Nabarro–Herring creep, J. Mech. Phys. Solids 44 (1996) 1429.
[5] A.C.F. Cocks, S.P.A. Gill, A variational approach to two dimensional grain-growth, I. Theory, Acta Metall. 44 (1996) 4765–4775.
[6] A.C.F. Cocks, J. Pan, Void growth ahead of a dominant crack in a material which deforms by Coble creep, Int. J. Fract. 60 (1993) 249–265.
[7] A.C.F. Cocks, A.A. Searle, Cavity growth in ceramic materials under multiaxial stress states, Acta Metall. 38 (1989) 2493.
[8] A.C.F. Cocks, S.P.A. Gill, J. Pan, Modelling microstructure evolution in engineering materials, Adv. Appl. Mech. 36 (1999) 81–162.
[9] C. Herring, Surface tension as a motivation for sintering, in: W.E. Kingston (Ed.), The Physics of Powder Metallurgy, McGraw-Hill, New York, 1955.
[10] M. Hillert, Acta Metall. 13 (1965) 227.
[11] S. Kucherenko, J. Pan, J.A. Yeomans, A combined finite element and finite difference scheme for computer simulation of microstructure evolution and its application to pore-boundary separation during sintering, Comput. Mater. Sci. 18 (2000) 76–92.
[12] W.W. Mullins, Theory of thermal grooving, J. Appl. Phys. 28 (1957) 333–339.
[13] W.W. Mullins, Mass transport at interfaces in single component systems, Met. Mat. Trans. A 26A (1995) 1917.
[14] A. Needleman, J.R. Rice, Plastic creep flow effects in the diffusive cavitation of grain boundaries, Acta Metall. 28 (1980) 1315–1332.
[15] J. Pan, Modelling sintering at different length scales, Int. Mater. Rev. 48 (2) (2003) 1–17.
[16] J. Pan, A.C.F. Cocks, Numerical simulation of superplastic deformation, Comput. Mater. Sci. 1 (1993) 95–109.
[17] J. Pan, A.C.F. Cocks, A numerical technique for the analysis of coupled surface and grain-boundary diffusion, Acta Mater. 43 (1995) 1395–1406.
[18] J. Pan, A.C.F. Cocks, S. Kucherenko, Finite element formulation of coupled grain-boundary and surface diffusion with grain-boundary migration, Proc. Roy. Soc., London A 453 (1997) 2161–2184.
[19] J. Pan, H.N. Ch'ng, A.C.F. Cocks, Sintering kinetic of large pores, Mech. Mater. (2003), submitted. Also see PhD thesis 'A numerical study of microstructural evolution during solid state sintering' by H.N. Ch'ng, May 2003, University of Surrey.
[20] J. Pan, H. Le, S. Kucherenko, J.A. Yeomans, A model for the sintering of spherical particles of different sizes, Acta Mater. 46 (1998) 4671–4690.
[21] B. Sun, Z. Suo, W. Yang, A finite element method for simulating interface motion, part 1: migration of phase and grain-boundaries, Acta Mater. 45 (5) (1997) 1907–1915.
[22] Z. Suo, Motions of microscopic surfaces in materials, Adv. Appl. Mech. 33 (1997) 193–294.
[23] Z. Suo, Z. Wang, Diffusive void bifurcation in stressed solid, J. Appl. Phys. 76 (1994) 3410–3421.
[24] W. Zhang, J.H. Schneibel, The sintering of two particles by surface and grain-boundary diffusion – a two-dimensional study, Acta Metall. 43 (1995) 4377.
[25] W. Zhang, P. Sachenko, J.H. Schneibel, I. Gladwell, Coalescence of two particles with different sizes by surface diffusion, Phil. Mag. A 82 (2002) 2995–3011.